Dioxygenases without Requirement for Cofactors and Their Chemical Model Reaction: Compulsory Order Ternary Complex Mechanism of 1*H*-3-Hydroxy-4-oxoquinaldine 2,4-Dioxygenase Involving General Base Catalysis by Histidine 251 and Single-Electron Oxidation of the Substrate Dianion†

Ursula Frerichs-Deeken,‡,§ Kalina Ranguelova,⊥ Reinhard Kappl,⊥ Jürgen Hüttermann,⊥ and Susanne Fetzner*,‡

Institut für Molekulare Mikrobiologie und Biotechnologie, Westfälische Wilhelms-Universität Münster, D-48149 Münster, Germany, AG Mikrobiologie, Institut für Chemie und Biologie des Meeres, Carl von Ossietzky Universität Oldenburg, D-26111 Oldenburg, Germany, and Fachrichtung Biophysik und Physikalische Grundlagen der Medizin, Universität des Saarlandes, D-66421 Homburg, Germany

Received June 18, 2004; Revised Manuscript Received September 8, 2004

ABSTRACT: 1*H*-3-Hydroxy-4-oxoquinaldine 2,4-dioxygenase (Hod) is a cofactor-less dioxygenase belonging to the α/β hydrolase fold family, catalyzing the cleavage of 1*H*-3-hydroxy-4-oxoquinaldine (**I**) and 1*H*-3-hydroxy-4-oxoquinoline (**II**) to *N*-acetyl- and *N*-formylanthranilate, respectively, and carbon monoxide. Bisubstrate steady-state kinetics and product inhibition patterns of HodC, the C69A protein variant of Hod, suggested a compulsory-order ternary-complex mechanism, in which binding of the organic substrate precedes dioxygen binding, and carbon monoxide is released first. The specificity constants, $k_{cat}/K_{m,A}$ and $k_{cat}/K_{m,O_2}$, were 1.4×10^8 and 3.0×10^5 M^{-1} s^{-1} with **I** and 1.2×10^5 and 0.41×10^5 M^{-1} s^{-1} with **II**, respectively. Whereas HodC catalyzes formation of the dianion of its organic substrate prior to dioxygen binding, HodC-H251A does not, suggesting that H251, which aligns with the histidine of the catalytic triad of the α/β hydrolases, acts as general base in catalysis. Investigation of base-catalyzed dioxygenolysis of **I** by electron paramagnetic resonance (EPR) spectroscopy revealed formation of a resonance-stabilized radical upon exposure to dioxygen. Since in D_2O spectral properties are not affected, exchangeable protons are not involved, confirming that the dianion is the reactive intermediate that undergoes single-electron oxidation. We suggest that in the ternary complex of the enzyme, direct single-electron transfer from the substrate dianion to dioxygen may occur, resulting in a radical pair. Based on the estimated spin distribution within the radical anion (observed in the model reaction of **I**), radical recombination may produce a C4- or C2-hydroperoxy(di)anion. Subsequent intramolecular attack would result in the 2,4-endoperoxy (di)-anion that may collapse to the reaction products.

1*H*-3-Hydroxy-4-oxoquinaldine 2,4-dioxygenase (Hod)[1] from *Arthrobacter ilicis* Rü61a and 1*H*-3-hydroxy-4-oxoquinoline 2,4-dioxygenase (Qdo) from *Pseudomonas putida* 33/1 are involved in the anthranilate pathway of quinaldine and 4-quinolone degradation, respectively. They catalyze the insertion of dioxygen at C2 and C4 of their *N*-heteroaromatic substrates, resulting in cleavage of two carbon−carbon bonds and release of carbon monoxide (Scheme 1, part A). In contrast to almost all other known oxygenases, these bacterial 2,4-dioxygenases neither contain nor require any cofactor or metal ion for catalysis (for a review, see ref *1*). The uniqueness of Qdo and Hod is corroborated by the finding that their amino acid sequences do not share similarities with known oxygenases (*2*). Instead, sequence analysis and secondary structure predictions of Hod (a 32 kDa monomer) and Qdo (a 30 kDa monomer) classify them as belonging to the family of the α/β hydrolases within the superfamily of the α/β hydrolase fold (*3*). This large enzyme family mainly comprises hydrolases with diverse catalytic functions (*4*, *5*). The bacterial 2,4-dioxygenases Qdo and Hod and luciferase (luciferin:oxygen 2-oxidoreductase (decarboxylating)) from the anthozoan coelenterate *Renilla reniformis* (*6*, *7*), which catalyzes the bioluminescent oxidation of an imidazolopyrazinone-type luciferin, apparently are the only oxygenases within the α/β hydrolase fold proteins.

The catalytic residues of the α/β hydrolases usually form a triad consisting of a nucleophilic residue found within the "nucleophile elbow" consensus motif Sm-X-Nu-X-Sm-Sm (where Sm is a small amino acid, Nu is the nucleophile, and X denotes any amino acid), a highly conserved histidine, and an acidic residue (*4*, *5*). Both Hod and Qdo actually contain a conserved histidine residue that aligns with the triad

† Supported by the Deutsche Forschungsgemeinschaft (Grants FE 383/5-1 and FE 383/5-2).

* Corresponding author. Mailing address: Institut für Molekulare Mikrobiologie und Biotechnologie, Westfälische Wilhelms-Universität Münster, Corrensstrasse 3, D-48149 Münster, Germany. Phone: +49 (0) 251/83 39824. Fax +49 (0) 251/83 38388. E-mail: fetzner@uni-muenster.de. URL: http://mibi1.uni-muenster.de/Fetzner/index.htm.

‡ Westfälische Wilhelms-Universität Münster.

§ Carl von Ossietzky Universität Oldenburg.

⊥ Universität des Saarlandes.

[1] Abbreviations: BMPO, 5-*tert*-butoxycarbonyl 5-methyl-1-pyrroline *N*-oxide; DMF, *N*,*N*-dimethylformamide; EPR, electron paramagnetic resonance; Hod, 1*H*-3-hydroxy-4-oxoquinaldine 2,4-dioxygenase; HodC, C69S mutant of Hod; PA, polyacrylamide; Qdo, 1*H*-3-hydroxy-4-oxoquinoline 2,4-dioxygenase; ^{t}BuOK, potassium *tert*-butoxide.

10.1021/bi048735u CCC: $27.50
Published on Web 10/21/2004

Scheme 1: Reactions Catalyzed by Bacterial 2,4-Dioxygenases and Compounds Used[a]

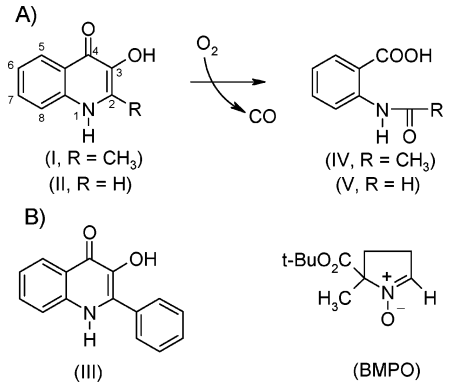

[a] Part A shows reactions catalyzed by bacterial 2,4-dioxygenases: 1*H*-3-hydroxy-4-oxoquinaldine 2,4-dioxygenase (Hod, substrate **I**) and 1*H*-3-hydroxy-4-oxoquinoline 2,4-dioxygenase (Qdo, substrate **II**); (**I**) 1*H*-3-hydroxy-4-oxoquinaldine; (**II**) 1*H*-3-hydroxy-4-oxoquinoline; (**IV**) *N*-acetylanthranilic acid; (**V**) *N*-formylanthranilic acid. Part B shows 1*H*-3-hydroxy-4-oxo-2-phenylquinoline (**III**) and 5-*tert*-butoxycarbonyl 5-methyl-1-pyrroline *N*-oxide (BMPO). The atom numbering of the quinoline ring follows the recommendation of the IUPAC Commission on the Nomenclature of Organic Chemistry (*25*).

histidine of the α/β hydrolases and a serine residue as potential nucleophile that is conserved within a motif corresponding to the signature sequence of the "nucleophile elbow" (*2*). Site-directed mutagenesis of the 2,4-dioxygenase Qdo was used to assess the catalytic relevance of these amino acid residues. The conserved histidine residue H244 of Qdo indeed was found to be catalytically essential. However, because the S95A variant of Qdo still showed activity (with an apparent k_{cat} of 7.4% of that of the native enzyme), the role of the conserved serine residue is not clear. It might be involved in catalysis, but it is not absolutely essential for the reaction to occur. Moreover, our previous efforts to identify a catalytically relevant acidic residue that might represent the third amino acid of a possible triad have failed. We thus have suggested that the 2,4-dioxygenases do not contain a "canonical" catalytic triad (*2*, *8*).

Apart from the 2,4-dioxygenases Qdo and Hod (and presumably *Renilla* luciferase), only few examples of other cofactor-less oxygenases have been reported, which however do not share sequence similarity with Qdo and Hod and belong to separate enzyme families. Urate oxidase catalyzes a reaction between urate and dioxygen to form urate hydroperoxide as a catalytic intermediate, without involvement of any prosthetic group or metal ion (*9*, *10*). The reaction has been proposed to involve direct single-electron transfer from the urate dianion to dioxygen (*9*, *11*). Quinone-forming monooxygenases also do not contain or require any cofactor; they are found in several *Streptomyces* species as "tailoring enzymes" in the biosynthesis of several aromatic polyketide antibiotics (*1* and references therein, *12*).

A fundamental problem in the dioxygenation of organic compounds is that a direct reaction of triplet-state dioxygen with a singlet-state organic molecule to form singlet products would violate the spin conservation rule, that is, it is a low-probability or high-energy process. Ground-state dioxygen therefore has to be activated by changing its spin configuration. Many dioxygenases use a paramagnetic metal center to mediate the triplet to singlet interconversion, producing a metal-bound activated oxygen species (*13*). Oxygenases that are devoid of any prosthetic group or cofactor present the mechanistically intriguing problem of how dioxygen is activated for catalysis. However, one solution to this problem is for the reaction to proceed via single electron-transfer steps, as assumed for the reaction of reduced flavins and pterins with dioxygen.

It is generally believed that transfer of one electron from the anion of the reduced flavin or pterin to dioxygen forms a semiquinone−superoxide radical pair that under spin inversion recombines to the corresponding hydroperoxide (*14*, *15*). However, such a mechanism can be expected to be possible only for organic substrates (anions) that easily undergo a one-electron oxidation, forming resonance-stabilized radicals. It may be interesting to note that one-electron oxidation of the imidazolopyrazinone luciferin anion with molecular oxygen to produce a radical pair has been discussed for the *Cypridina* luciferin 36 years ago (*16*) and may also be assumed for the structurally related *Renilla* luciferin. The initial reaction of the luciferin (anion) with dioxygen is thought to form a C2-hydroperoxy anion and thus proceeds analogous to the reaction of flavins or pterins with dioxygen (*16*).

In a first approach to better understand the function of cofactor-less 2,4-dioxygenases, we have examined the steady-state kinetic properties of Hod. The order of substrate binding and product release was deduced from product inhibition studies. Based on substrate binding experiments, we propose that formation of the 1*H*-3-hydroxy-4-oxoquinaldine dianion by histidine 251 as general base is the first step in catalysis. Single-electron oxidation of the 1*H*-3-hydroxy-4-oxoquinaldine dianion to form a resonance-stabilized radical anion was observed under oxic conditions for a base-catalyzed model reaction that mimicks enzyme-catalyzed dioxygenolysis. We suggest a catalytic mechanism for cofactor-less 2,4-dioxygenases Hod and Qdo involving single-electron transfer from substrate dianion to dioxygen. Besides the known reactivity of carbanions toward molecular oxygen (*17*) and the well-studied flavin and pterin oxygenation reactions, the enzymatic reactions discussed in this work suggest that direct reaction of (enzyme-bound) anionic intermediates with dioxygen are more common in nature than generally assumed.

MATERIALS AND METHODS

Materials. 1*H*-3-Hydroxy-4-oxoquinaldine (**I**) was synthesized from 3-formyl-2-methyl-4(1*H*)-quinolone (*18*) as described by Cornforth and James (*19*). 1*H*-3-Hydroxy-4-oxoquinoline (**II**) was synthesized according to Evans and Eastwood (*20*). 3-Benzyloxy-2-methyl-4-pyrone, synthesized according to Harris (*21*), was used as the reactant for the synthesis of 3-hydroxy-2-methyl-1*H*-pyridine-4-one (*22*). 1*H*-3-Hydroxy-4-oxo-2-phenylquinoline (**III**; Scheme 1, part B) and *N*-formylanthranilate were synthesized as described in refs *23* and *24*, respectively. DEAE Sephacel was from Amersham Biosciences, Freiburg, Germany. Bio-Gel hydroxyapatite HT, and the columns UNO Q6 and Bio-Prep SE 1000/17 were from Bio-Rad Laboratories, Munich, Germany. 5-*tert*-Butoxycarbonyl 5-methyl-1-pyrroline *N*-oxide (BMPO; Scheme 1, part B) was generously provided by B. Kalyanaraman, The Medical College of Wisconsin, Milwaukee, WI. Dioxygen (99.995%), dinitrogen (99.99%), carbon monoxide (99%), and argon (99.998%) were from

Messer Griesheim, Krefeld, Germany. All other chemicals were obtained from commercial sources and were of the highest purity available. The atom numbering of the quinoline ring follows the recommendation of the IUPAC Commission (*25*).

Bacterial Strains, Plasmids, and Growth Conditions. A. ilicis Rü61a (*26*) was grown in Luria−Bertani (LB) medium (*27*) at 30 °C. *Escherichia coli* M15(pREP4) (Qiagen, Hilden, Germany) was used as a host for recombinant pQE50 (Qiagen) and for protein expression. *E. coli* XL1-Blue MRF′ (*28*) was used as a host for derivatives of pQE50::*hod* constructed by site-directed mutagenesis. *E. coli* clones were grown in LB broth at 37 °C, either in the presence of kanamycin (50 μg/mL) and ampicillin (100 μg/mL) for cells harboring pQE50 or derivatives, as well as pREP4, or in the presence of ampicillin (100 μg/mL) for *E. coli* XL-1 Blue cells. Competent *E. coli* cells were prepared as described by Iwasaki et al. (*29*).

DNA Techniques, and Construction and Engineering of pQE50::hod. Genomic DNA of *A. ilicis* Rü61a was isolated according to Hopwood et al. (*30*). Plasmid DNA was prepared with the Plasmid Miniprep Kit (I) (peqLab Biotechnologie GmbH, Erlangen, Germany) as specified by the supplier. Agarose gel electrophoresis, restriction digestion, and DNA ligation were carried out using standard protocols (*27*). PCR with *Pfu* DNA polymerase (Promega, Mannheim, Germany) was performed according to the manual provided by the manufacturer.

The *hod* gene (EMBL accession no. AJ537472) was amplified from genomic DNA of *A. ilicis* Rü61a using the following primers: *hod-Bam*HI (5′-TCATGGTACCGGATC-C*ATG*ACCGACACATATCTGCATGAAACGC-3′) and *hod-Sal*I (5′-TTAATCCCGGGTCGACGGGAAG*TTA*CTG-GCCTTGGCGGATTGCC-3′) (restriction sites are underlined; start and stop triplets of *hod* are in italics). After digestion with *Bam*HI and *Sal*I, the amplificate was inserted into the *Bam*HI/*Sal*I restriction site of the expression vector pQE50 to generate pQE50::*hod* (*31*). Transformation of competent *E. coli* M15 [pREP4] cells with pQE50 derivatives was performed by electroporation (*32*).

For the deletion of vector fragments flanking the *hod* gene, pQE50::*hod* was used as template for *Pfu* polymerase-mediated amplification. The primers *hodstartfor* (5′-P-ATGACCGACACATATCTGCATG-3′) and *hodstartrev* (5′-P-AGTTAATTTCTCCTCTTTAATGAATTCTG-3′) were used to delete a 12 bp fragment upstream of *hod*, resulting in the plasmid pQE50m1−*hod*. The deleted fragment encloses the start codon provided by the plasmid, and a potential ribosome binding site. For the deletion of a 33 bp DNA fragment downstream of the *hod* insert that is located between the stop codon of *hod* and the plasmid-derived stop codon, the primers *hodstopfor* (5′-P-TTACTGGCCTTG-GCGGATTG-3′) and *hodstoprev* (5′-P-TGAGCTTGGACTC-CTGTTGATAGATC-3′) and the template pQE50m1−*hod* were used, generating pQE50m2−*hod*.

Oligonucleotide Site-Directed Mutagenesis of pQE50m2−hod. Site-directed mutagenesis was performed using Stratagene's QuikChange protocol. For replacement of C69 by serine, plasmid pQE50m2−*hod* served as template for *Pfu* polymerase-mediated amplification with the primer *hodC69S* (5′-GGTCACGGACTCTCGCCCTCCGAGGTC-CCAGACTTTGGC-3′), resulting in pQE50m2−*hodC69S*. The HodC69S protein was designated HodC. The replacement in HodC of H251 by alanine was achieved using pQE50m2−*hodC69S* as template, and the primer *hodH251A* (5′-GGCGGGCCGACCGCCTTCCCCGCCATC-3′) (altered codons are underlined). All deletions and mutations were confirmed by sequence analysis of DNA fragments encompassing the mutations (MWG-Biotech, Ebersberg, Germany).

Expression and Purification of Recombinant Hod. Growth of *E. coli* M15 (pREP4) clones harboring recombinant pQE50::*hod* or derivatives, induction of protein expression, and preparation of crude cell extracts were performed as described for clones containing pQE30::*qdo* (*8*), except that Tris-HCl buffer (buffer A, 50 mM Tris-HCl, pH 8.0, 2 mM EDTA) was used to prepare crude extracts. Purification of Hod proteins was performed at room temperature unless indicated otherwise. Purification procedure 1 is a modification of the method described by Bauer et al. (*33*). Crude cell extract was applied to DEAE Sephacel packed into a Bio-Scale MT6 column (Bio-Rad) equilibrated in buffer A. The column was washed with the same buffer, then with buffer A containing 0.1 M KCl, and finally proteins were desorbed with a linear gradient (50 mL) from 0.1 to 0.4 M KCl in buffer A (1 mL/min). Active fractions were combined and washed by ultrafiltration (molecular mass cutoff 10 kDa) with 10 mM potassium phosphate buffer, pH 7.0 (buffer B). The concentrated protein solution was applied to hydroxyapatite (1 cm × 5 cm column) equilibrated in buffer B. Hod did not adsorb to hydroxyapatite and was eluted by washing the column with buffer B (0.75 mL/min). The eluate was washed by ultrafiltration with buffer A and applied to an UNO Q6 column equilibrated in the same buffer. After washing the column with buffer A containing 0.1 M KCl, the protein was eluted with a linear gradient (30 mL) from 0.1 to 0.4 M KCl in buffer A (1 mL/min). The concentrated protein preparation was subjected to gel filtration on Bio-Prep SE 1000/17 using buffer A (0.1 mL/min). Active fractions were pooled, concentrated by ultrafiltration, and stored at −80 °C.

For purification procedure 2, crude cell extract was applied to a DEAE Sephacel column and eluted as described in purification procedure 1. The combined active fractions were washed with buffer A. The concentrated protein was subjected to preparative polyacrylamide gel electrophoresis in a model 491 prep cell (Bio-Rad Laboratories). Electrophoresis under nondenaturing conditions was performed in a 12.8% T/0.33% C resolving gel with a 4.3% T/0.11% C stacking gel using the "high-pH discontinuous" buffer system as described by Hames (*34*). The protein was eluted at a flow rate of 0.9 mL/min. Active fractions were combined, concentrated, washed with buffer A, and stored at −80 °C.

Protein Determination. Protein concentrations were estimated by the method of Bradford as modified by Zor and Selinger (*35*) using bovine serum albumin as standard.

Analytical Polyacrylamide Gel Electrophoresis. The purity of protein preparations was assessed by SDS−PAGE and by nondenaturing high-pH PA gels (*34*) using 12.8% T/0.33% C and 4.3% T/0.11% C in the resolving and stacking gel, respectively. Proteins were stained with Coomassie blue G-250 (0.2% [w/v] in aqueous trichloroacetic acid [50%, w/v]).

Steady-State Kinetics. The activity of Hod variants was determined spectrophotometrically by measuring substrate

consumption using molar extinction coefficients of $\epsilon_{334\ nm} = 9570\ M^{-1}\ cm^{-1}$ (**I**) and $\epsilon_{337\ nm} = 10\,500\ M^{-1}\ cm^{-1}$ (**II**). One unit of enzyme activity was defined as the amount of enzyme required to consume 1 μmol of **I** or **II** per minute at 30 °C in the standard assay (980 μL of buffer A, 10 μL of the appropriate dilution of enzyme preparation, and 10 μL **I** or **II** [10 mM in ethanol]). Bisubstrate steady-state experiments were performed by varying the concentration of one substrate in the presence of different, constant concentrations of the second substrate. For product inhibition studies, the concentration of one substrate and one of the products was kept constant, while the concentration of the second substrate was varied.

Stock solutions and enzyme solutions were repeatedly evacuated and reequilibrated in N_2/H_2 (90%/10%) atmosphere, kept under argon, and withdrawn using a gastight syringe. Buffers were brought to the temperature of reaction before equilibrating them in appropriate gas mixtures; enzyme samples were kept on ice. For reactions with dissolved O_2 concentrations other than that of air-saturated buffer (230 μM dissolved O_2 at 30 °C (*36*)), buffer was saturated at 30 °C with appropriate mixtures of humidified O_2 and N_2 gas for 30 min prior to use. The concentrations of dioxygen in the assays were calculated on the basis of its solubility in water at 30 °C and the percent by volume concentration of O_2 in the atmosphere used to equilibrate the buffer. For product inhibition studies, humidified CO gas was added to the gas mixture. The concentration of CO in buffer bubbled with 100% CO was presumed to be 882 μM at 30 °C (*37*). With a gastight syringe, the equilibrated buffers were added to a cuvette previously flushed with argon. The enzyme, and if required the product *N*-formylanthranilate, were added under argon atmosphere. All reactions were initiated by injecting the organic substrate **I** or **II** after equilibrating the assay mixture for 20 s.

Analysis of Kinetic Data. Data were analyzed graphically, by calculations using the least-squares fitting and dynamic weighting options of LEONORA (*38*), or both. For the determination of apparent kinetic constants (variation of only one substrate), initial velocities (v_i) were fitted to the Michaelis−Menten equation (eq 1) or to the equivalent

$$v_i = \frac{V^{app}[S]}{K_{m,S}^{app} + [S]} \quad (1)$$

equation describing a mechanism that involves substrate inhibition (eq 2). When two substrate concentrations were

$$v_i = \frac{V^{app}[S]}{K_{m,S}^{app} + [S] + [S]^2/K_{si,S}^{app}} \quad (2)$$

varied, initial velocity data were fitted to equations describing a substituted (ping-pong) mechanism (eq 3), a ternary

$$v_i = \frac{V[A][O_2]}{K_{m,O_2}[A] + K_{m,A}[O_2] + [A][O_2]} \quad (3)$$

complex mechanism (eq 4), and a ternary complex mechanism with substrate inhibition (eq 5). Initial velocity data of

$$v_i = \frac{V[A][O_2]}{K_{s,A} + K_{m,O_2}[A] + K_{m,A}[O_2] + [A][O_2]} \quad (4)$$

$$v_i = \frac{V[A][O_2]}{K_{s,A} + K_{m,O_2}[A] + K_{m,A}[O_2](1 + [A]/K_{si,A}) + [A][O_2]} \quad (5)$$

product inhibition studies were fitted to equations for competitive, uncompetitive, and noncompetitive inhibition (eqs 6−8). In these equations, initial concentrations of

$$v_i = \frac{V^{app}[S]}{K_{m,S}^{app}(1 + [I]/K_{i,c}^{app}) + [S]} \quad (6)$$

$$v_i = \frac{V^{app}[S]}{K_{m,S}^{app} + [S](1 + [I]/K_{i,u}^{app})} \quad (7)$$

$$v_i = \frac{V^{app}[S]}{K_{m,S}^{app}(1 + [I]/K_{i,c}^{app}) + [S](1 + [I]/K_{i,u}^{app})} \quad (8)$$

substrate and products are represented by the symbols in square brackets. The symbols A, O_2, and I are used for the aromatic substrate, molecular dioxygen, and inhibitor, respectively. S is used for a single varied substrate. In the determination of apparent kinetic constants, S is exchanged by A when the aromatic substrate was varied and by O_2 when molecular oxygen was varied. K_m refers to the Michaelis constant, $K_{s,A}$ is the equilibrium dissociation constant of the enzyme substrate complex (EA), K_{si} is the substrate inhibition constant, and K_i is the inhibition constant. The competitive and the uncompetitive inhibition constants are denoted by $K_{i,c}$ and $K_{i,u}$, respectively. The limiting rate V is related to the catalytic constant k_{cat} through the equation $k_{cat} = V/(60s[e_0])$ with $[e_0]$ equal to the enzyme concentration used in the assay.

UV/Visible Spectroscopy. UV/visible spectra were recorded on an UV/vis spectrophotometer Pharmacia LKB Autofill III. To determine the pK_a values of 1*H*-3-hydroxy-4-oxoquinaldine (**I**) and 1*H*-3-hydroxy-4-oxoquinoline (**II**), UV/vis spectra of **I** or **II** (50 μM) adjusted to different pH values with NaOH or HCl were recorded at 25 °C, under oxic and anoxic conditions. Anoxic conditions were achieved by bubbling the solutions with argon for at least 20 min. Spectra were recorded using a gastight cuvette. The range of pH was from 1.0 to 13.0, with increments of 1.0 pH units. Absorbance spectra of HodC, substrate (**I**), organic product (*N*-acetylanthranilate), equimolar mixtures of HodC with **I** or with *N*-acetylanthranilate, and an equimolar mixture of HodC-H251A and **I** were recorded in 50 mM Tris-HCl, pH 8.0, at 25 °C. All solutions were flushed with argon for 20 min and incubated for 2 h in an anaerobic glovebox under an inert atmosphere (N_2/H_2, 90%/10%) prior to mixing in a gastight cuvette. The final concentrations of HodC, HodC-H251A, and **I** were 50 μM each. After monitoring the UV/vis spectrum under anoxic conditions (for up to 1.5 h), each

sample was flushed with air for 1 min, and the spectrum was recorded again.

Base-catalyzed dioxygenolysis of **I** or **II** in DMF, using ^{t}BuOK as catalyst, yields the same products as the enzyme-catalyzed reactions (*33*). The reaction also proceeds in aqueous NaOH (*31*). Base-catalyzed dioxygenolysis of **III** was recently described by Czaun and Speier (*39*). The UV/vis absorption spectra of **I**, **II**, and **III** in DMF and in H_2O with ^{t}BuOK or NaOH were recorded under oxic and anoxic conditions. Anoxic conditions were adjusted by bubbling the solutions with argon for 30 min prior to mixing in a gastight, argon-flushed cuvette. The assays contained 100 nmol of **I**, **II**, or **III** and 177 μmol of ^{t}BuOK or 200 μmol of NaOH in 1 mL of DMF or H_2O.

EPR Spectroscopy. For the model reactions, 500 μL-aliquots of substrate (0.13 M) and base (0.13 M) were prepared in an anaerobic glovebox (Coy) with degassed solvents (DMF or 50 mM Tris-HCl, pH 8). From each batch, 100 μL was taken and mixed inside the glovebox in an Eppendorf vessel, formally yielding equimolar concentrations. The mixture was subsequently transferred to a 100 μL flat cell (Wilmad), which was then removed from the glovebox. During EPR measurement in a TMH 8603 cavity (Bruker), a minor leakage of air into the anoxic flat cell was observed in some cases. Small amounts of air were allowed to enter the flat cell by shortly opening the top stopper. For full exposure to air, the reaction mixture was transferred from the flat cell into an open Eppendorf vessel, reacted for 5−10 min and then refilled into the flat cell. In case of incomplete solubility of substrates or base (in buffer), the solutions were stirred for several minutes inside the glovebox, and the supernatant was transferred into the flat cell. In such cases, nonequimolar concentrations prevailed after mixing the 100 μL aliquots. The spin trap BMPO was added under anoxic conditions to the 500 μL aliquots of substrate solution to a final concentration of 3.09 M before mixing with the base. In all cases control experiments under anoxic or oxic conditions were performed to monitor signals appearing in substrate or base solutions prior to mixing. EPR experiments were performed on a Bruker ESP 300E spectrometer equipped with a frequency counter and a NMR-gaussmeter. Spectra were recorded at microwave powers of 20, 2, or 0.2 mW using a modulation amplitude of 0.1 or 0.5 G (1 G = 0.1 mT). Other parameters such as receiver gain and field sweep were usually kept constant within a series. Depending on the signal intensities, spectra accumulation was necessary to achieve a reasonable signal-to-noise ratio. Spectra presented in the figures are normalized in this respect. For the reaction of enzyme with substrate with or without BMPO, the following concentrations were used: $C_{enzyme} = 3.7$ mM; $C_{substrate} = 1.19$ M; $C_{BMPO} = 3.09$ M. Again control experiments were performed under identical conditions. The EPR spectra were simulated with the Simfonia and Xsophe software tools (Bruker) particularly taking advantage of the iteration routine implemented in the Xsophe program.

RESULTS

Homogeneity of Hod and HodC Preparations. Preparations of Hod from *E. coli* pQE50::*hod* (obtained by protocol 1) consisted of several monomeric and dimeric forms of about 32 and 64 kDa, respectively (Figure 1, lane 1). Separation into four different monomeric and at least two different dimeric forms was achieved by preparative native PAGE. Each of the monomeric forms was catalytically active; however the monomers slightly differed in their molecular masses as indicated by matrix-assisted laser desorption ionization time-of-flight mass spectrometry (MALDI-TOF-MS, data not shown), indicating that the expression clone produced several different Hod protein variants. The purified monomers showed an inclination toward dimerization even in the presence of 1,4-dithio-D,L-threitol.

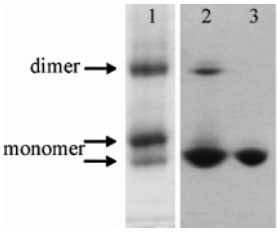

FIGURE 1: Native PAGE of recombinant Hod proteins: Hod from *E. coli* M15(pREP4) pQE50::*hod* (lane 1) and *E. coli* M15(pREP4) pQE50m2-*hod* (lane 2); HodC from *E. coli* M15(pREP4) pQE50m2-*hod*C69S (lane 3). Hod proteins in lanes 1 and 2 were purified according to protocol 1; HodC was prepared according to protocol 2.

Using site-directed mutagenesis, we deleted two vector-derived fragments flanking the inserted *hod* gene, namely, a 12 bp sequence upstream of the *hod* start codon containing a vector-derived start codon, and a 33 bp downstream sequence located between the *hod* stop codon and a vector-derived stop codon. The latter mutation resulted in a direct in-frame coupling of the two stop codons. The resulting clone, *E. coli* M15(pREP 4) pQE50m2-*hod*, indeed produced a single monomeric form of Hod, which however also dimerized upon concentration (Figure 1, lane 2). Replacement of C69 by serine prevented the formation of dimers and allowed the expression and purification (protocol 2) of the HodC protein to homogeneity (Figure 1, lane 3). The amount of HodC obtained from 2.3 g of wet cell paste was 7.4 mg. Electrophoretically pure HodC showed a specific activity of 70 U/mg, comparable to that of the wild-type enzyme, and was used for the kinetic and spectroscopic studies described below.

*Steady-State Kinetic Studies of HodC Using the Physiological Substrate 1H-3-Hydroxy-4-oxoquinaldine (**I**).* For steady-state kinetics of HodC, concentrations of **I** from 2 to 200 μM were used, representing the photometrically measurable range. At concentrations of **I** above 40 μM, inhibition of the enzyme was obvious when the experiment was performed in air-saturated buffer (230 μM O_2). Fitting the initial velocity data to eqs 1 and 2 yielded similar kinetic parameters; however, the data showed a slightly better fit to eq 2, which takes inhibition by the aromatic substrate into consideration; $K_{si,A}^{app}$ was 907 ± 109 μM (Table 1). The effect of inhibition through substrate **I** depends on the dioxygen concentration. No inhibition was observed when the experiment was performed in buffer containing concentrations of O_2 higher than 241 μM; at these dioxygen concentrations, data fits to eq 2 resulted in negative values for $K_{si,A}^{app}$.

A remarkable increase of k_{cat}^{app} for **I** from 35 ± 1 to 145 ± 3 s^{-1} was observed when the dioxygen concentration was increased from 120 to 964 μM, clearly indicating a rate-

Table 1: Apparent Steady-State Kinetic Parameters of HodC Using 1*H*-3-Hydroxy-4-oxoquinaldine (**I**) and 1*H*-3-Hydroxy-4-oxoquinoline (**II**) as Varied Substrates[a]

substrate	equation	$K_{m,A}^{app}$ (μM)	k_{cat}^{app} (s^{-1})	$K_{si,A}^{app}$ (μM)	$k_{cat}^{app}/K_{m,A}^{app}$ ($\times 10^6$ M^{-1} s^{-1})
I	1	1.3(0.1)[b]	51(1)		40(4)
I	2	1.5(0.1)[b]	54(1)	907(109)	36(3)
II	1	93(7)	7(0)		0.08(0.006)
II	2	185(46)	13(3)	179(79)	0.08(0.03)

[a] Experiments were performed using air-saturated (230 μM O_2) 50 mM Tris-HCl, pH 8.0, 2 mM EDTA, at 30°C. The values of the parameters and their standard errors (in parentheses) were calculated using the least-squares and dynamic weighting options of LEONORA (*38*). The data sets used to calculate the parameters contain 54 points. [b] These K_m values should be considered as estimations. Since the K_m values are rather low, the lowest substrate concentration that could be measured photometrically was 2-fold higher than the estimated K_m value.

limiting effect of the lower dioxygen concentration due to unsaturating conditions. At concentrations of **I** from 10 to 100 μM, k_{cat}^{app} for O_2 was constant at 228 $\pm$ 25 s^{-1} but was only 146 $\pm$ 29 s^{-1} at 2.5 μM **I** due to unsaturating conditions of **I** at concentrations below 10 μM.

In contrast to k_{cat}^{app} for **I**, the apparent Michaelis constants $K_{m,A}^{app}$ for **I**, as well as K_{m,O_2}^{app}, showed no significant correlation with the concentration of the respective other substrate: $K_{m,A}^{app}$ for **I** independent of the dioxygen concentration was 1.7 $\pm$ 0.6 μM, which is close to the detection limit of the enzyme assay, and K_{m,O_2}^{app} independent of the concentration of **I** was 805 $\pm$ 146 μM, which is close to the limit of oxygen solubility under atmospheric pressure.

Bisubstrate steady-state kinetics of HodC were measured by varying the concentration of one substrate at several constant concentrations of the other substrate. Concentrations of **I** from 2.5 to 100 μM and of O_2 from 120 to 1205 μM were used. Primary plots of [**I**]/v against [**I**] gave a series of lines with no common intersection point (data not shown), possibly due to the effect of substrate inhibition. Fitting the data to equations describing a ternary complex mechanism with and without substrate inhibition or a substituted mechanism (eqs 3−5) likewise could not discriminate between these mechanisms (Table 2). However, an accurate determination of the catalytic constants for **I** and O_2 was not possible because the estimated Michaelis constants, $K_{m,A}$ and K_{m,O_2}, are near the experimental limits. Apparent steady-state kinetic parameters of dioxygen were determined at saturating (>20 μM **I**) and unsaturating (<10 μM **I**) conditions, but for the apparent steady-state kinetic parameters of **I**, only nonsaturating concentrations of oxygen could be used.

Steady-State Kinetics with Alternative Substrates. When 3-hydroxy-2-methylpyran-4-one and 3-hydroxy-2-methyl-1*H*-pyridine-4-one were tested as possible alternative substrates, it turned out that neither of these compounds was accepted as substrate by HodC, nor did they act as inhibitors against the aromatic substrate **I** when tested in concentrations up to 1 mM. This suggests that the benzene moiety of the physiological substrate is a determinant of substrate specificity, maybe with an important role in substrate binding. Likewise, 1*H*-3-hydroxy-4-oxo-2-phenylquinoline (**III**), the C2-phenyl derivative of **II**, was not a substrate of HodC.

Alternatively, conversion by HodC of 1*H*-3-hydroxy-4-oxoquinoline (**II**), the physiological substrate of 1*H*-3-hydroxy-4-oxoquinoline 2,4-dioxygenase (Qdo) from *Pseudomonas putida* 33/1, was tested. In air-saturated buffer (230 μM O_2), the apparent kinetic parameters were calculated using **II** in concentrations of 10−200 μM in the standard enzyme assay. No significant substrate inhibition was observed for these concentrations of **II**. The initial rate data showed a slightly better fit to eq 1, which describes a mechanism without substrate inhibition, than to eq 2 describing a mechanism with substrate inhibition. However, the values obtained from fitting the data to eq 2 do not exclude the possibility of inhibition through high concentrations of **II** (Table 1). The calculated apparent Michaelis constants for **II** (in air-saturated buffer) and for dioxygen (at 60 μM **II**) were 93 $\pm$ 7 (Table 1) and 233 $\pm$ 63 μM, respectively. These values allowed the variation of both substrate concentrations around the apparent Michaelis constant of **II** and O_2 over practicable ranges but did not allow measurements at saturating substrate concentrations. Within O_2 concentrations from 55 to 602 μM, no influence on $K_{m,A}^{app}$ (60 $\pm$ 6 μM) appeared, and there also was no influence on K_{m,O_2}^{app} (178 $\pm$ 50 μM) through different concentrations of **II** (10−150 μM). No inhibition through substrate **II** (up to 150 μM) was obvious; however, saturating conditions were not achieved due to the low solubility of **II**. An increase of k_{cat}^{app} for **II** from 2.2 $\pm$ 0.2 to 22.0 $\pm$ 0.1 s^{-1} was observed when the dioxygen concentration was increased from 55 to 1204 μM, clearly indicating the rate-limiting effect of dioxygen due to unsaturating conditions. When the concentration of **II** was increased from 10 to 150 μM, k_{cat}^{app} for O_2 increased from 1.3 $\pm$ 0.3 to 5.3 $\pm$ 0.8 s^{-1} and did not reach a saturating level.

For bisubstrate steady-state kinetics of HodC with **II**, concentrations of **II** from 10 to 150 μM and O_2 concentrations from 55 to 274 μM were used. Primary plots of [**II**]/v against [**II**] gave a series of straight lines intersecting at a single point to the left of the [**II**] axis (Figure 2). This is consistent with a mechanism that proceeds through a ternary complex, that is, both substrates must remain associated with the enzyme before the first product is released. Initial velocity

Table 2: Kinetic Parameters of HodC Using the Substrate 1*H*-3-Hydroxy-4-oxoquinaldine (**I**)[a]

mechanism	$K_{si,A}$ (μM)	$K_{s,A}$ (μM)	$K_{m,A}$ (μM)	K_{m,O_2} (μM)	k_{cat} (s^{-1})	$k_{cat}/K_{m,A}$ ($\times 10^8$ M^{-1} s^{-1})	$k_{cat}/K_{m,O_2}$ ($\times 10^8$ M^{-1} s^{-1})
ternary complex (eq 4)		2.0(0.6)	2.0(1.2)	907(138)	274(30)	1.4	0.003
ternary complex with inhibition by A (eq 5)	−423(−151)	1.7(0.6)	1.1(0.9)	973(102)	261(22)	2.4	0.003
substituted (eq 3)			6.9(1.6)	1320(212)	350(46)	0.5	0.003

[a] Experiments were performed using 50 mM Tris-HCl, pH 8.0, 2 mM EDTA, at 30°C. The values of the parameters and their standard errors (provided in parentheses) were calculated using the least-squares and dynamic weighting options of LEONORA (*38*). The data sets used to calculate the parameters contain 420 points.

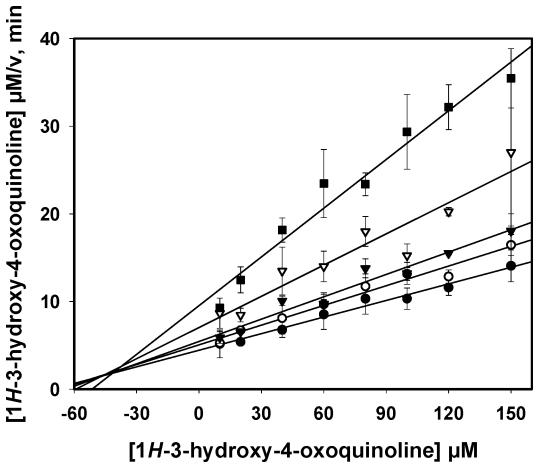

FIGURE 2: Hanes plots of initial rate data of the HodC-catalyzed 2,4-dioxygenolysis of 1*H*-3-hydroxy-4-oxoquinoline (**II**). Experiments were performed in 50 mM Tris-HCl, pH 8.0, 2 mM EDTA at 30 °C: 274 μM O_2 (●), 219 μM O_2 (○), 164 μM O_2 (▼), 110 μM O_2 (▽), and 55 μM O_2 (■).

data were fitted to the ternary-complex mechanism (eq 3) and the substituted-enzyme mechanism (eq 4). The results are summarized in Table 3. The best fit of the initial rate data is obtained for the equation that describes a ternary complex mechanism, a result that is in accordance with graphical predictions. We conclude that HodC-catalyzed 2,4-dioxygenolysis of **II** proceeds via formation of a ternary complex between the enzyme, its organic substrate, and dioxygen.

Product Inhibition Patterns. Product inhibition studies are commonly performed to determine whether there is a preferential order of substrate binding and product release for a particular multiple substrate reaction (*40*). Table 4 summarizes the results of the product inhibition of HodC. At nonsaturating levels of dioxygen (164 μM O_2), *N*-formylanthranilate was a competitive inhibitor versus **II**. This is indicative of the binding of *N*-formylanthranilate and **II** to the same enzyme form. When dioxygen was varied at nonsaturating levels of **II** (40 μM), *N*-formylanthranilate acts as a noncompetitive inhibitor versus O_2, indicating the binding to different enzyme forms. Carbon monoxide also is a noncompetitive inhibitor versus both dioxygen and substrate **II**; therefore, CO binds to a different enzyme form. This inhibition pattern rules out a "rapid equilibrium ordered bi bi", a "rapid equilibrium random bi bi", a "Theorell−Chance", or a substituted-enzyme mechanism. For HodC and 1*H*-3-hydroxy-4-oxoquinoline (**II**) as organic substrate, the inhibition patterns are consistent with a compulsory-order ternary-complex mechanism, in which binding of the aromatic substrate precedes dioxygen binding, and CO leaves the enzyme−product complex first, followed by release of *N*-formylanthranilate (Scheme 2).

Scheme 2: Mode of Substrate Binding and Product Release of 1*H*-3-Hydroxy-4-oxoquinaldine 2,4-Dioxygenase

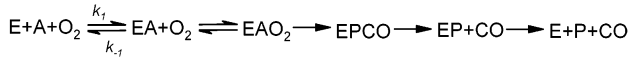

The specificity constant, $k_{cat}/K_{m,A}$, which is also the second-order rate constant (Scheme 2, k_1) for the association of the substrate **II** to HodC, was 1.2×10^5 M^{-1} s^{-1} (Table 3, eq 4). It is therefore 1170-fold lower than the specificity constant for the physiological substrate **I**, calculated to be 1.4×10^8 M^{-1} s^{-1} (Table 2). This value is close to diffusion control, ruling out the association of **I** to HodC as a rate-determining

Table 3: Kinetic Parameters of HodC Using 1*H*-3-Hydroxy-4-oxoquinoline (**II**) as Substrate[a]

mechanism	$K_{s,A}$ (μM)	$K_{m,A}$ (μM)	K_{m,O_2} (μM)	k_{cat} (s^{-1})	$K_{i,A}$ (μM)	$k_{cat}/K_{m,A}$ ($\times 10^5$ M^{-1} s^{-1})	$k_{cat}/K_{m,O_2}$ ($\times 10^5$ M^{-1} s^{-1})
ternary complex (eq 4)	45(15)	95(34)	270(91)	11(2)		1.2	0.41
ternary complex with inhibition by A (eq 5)	11(3)	125(24)	566(116)	13(2)	−379(−100)	1.0	0.30
substituted (eq 3)		1136(1370)	2811(3428)	75(88)			

[a] Experiments were performed using 50 mM Tris-HCl, pH 8.0, 2 mM EDTA, at 30°C. The O_2 concentration and the concentration of **II** were varied from 55 to 274 μM and 10 to 150 μM, respectively. The values of the parameters and their standard errors (provided in parentheses) were calculated using the least-squares and dynamic weighting options of LEONORA (*38*). The data sets used to calculate the parameters contain 160 points.

Table 4: Product Inhibition Pattern of HodC with 1*H*-3-Hydroxy-4-oxoquinoline (**II**)[a]

varied substrate	fixed substrate[b]	varied product	type of inhibition	$K_{i,c}^{app}$ (μM)	$K_{i,u}^{app}$ (μM)
II (20−180 μM)	O_2 (164 μM; unsaturated)	*N*-formylanthranilate (0−1000 μM)	competitive[c]	363(35)	
II (20−180 μM)	O_2 (438 μM)	*N*-formylanthranilate (0−1000 μM)	competitive[c]	324(20)	
O_2 (54−438 μM)	**II** (40 μM; unsaturated)	*N*-formylanthranilate (0−1000 μM)	noncompetitive[c]	445(78)	521(87)
II (20−180 μM)	O_2 (164 μM; unsaturated)	CO (0−588 μM)	noncompetitive[c]	1770(395)	1860(325)
II (20−180 μM)	O_2 (438 μM)	CO (0−588 μM)	uncompetitive[d]		503(41)
O_2 (54−438 μM)	**II** (40 μM; unsaturated)	CO (0−588 μM)	noncompetitive[d]	1238(914)	1068(304)

[a] Inhibition experiments were performed using 50 mM Tris-HCl, pH 8.0, 2 mM EDTA, at 30°C. The values of the parameters and their standard errors (provided in parentheses) were calculated using the least-squares and dynamic weighting options of LEONORA (*38*). [b] Because of the limited solubility of oxygen and of 1*H*-3-hydroxy-4-oxoquinoline (**II**), saturating conditions could not be investigated. [c] Slope and intercept replots versus inhibitor concentrations were linear. [d] Slope and intercept replots versus inhibitor concentrations were nonlinear.

step in 2,4-dioxygenolysis, but indicates that the methyl substituent at C2 of the substrate is important for efficient association with the enzyme. Since $K_{s,A} = k_{-1}/k_1$ represents the equilibrium dissociation constant of the enzyme substrate complex (EA), k_{-1} for the physiological substrate **I** was calculated to be 280 s^{-1} and that for substrate **II** to be 5 s^{-1}.

The specificity constant $k_{cat}/K_{m,O_2}$ for **I** was 3×10^5 M^{-1} s^{-1}; however, $k_{cat}/K_{m,O_2}$ for the alternative substrate **II** was 7.5-fold lower (0.4×10^5 M^{-1} s^{-1}), indicating slightly different reactivities of the bound substrates toward dioxygen.

Activity of HodC-H251A. Because H251 of Hod aligns with the histidine residue of the catalytic triad of the α/β hydrolases, its possible involvement in catalysis was investigated. Electrophoretically pure HodC-H251A, purified according to protocol 2, showed a specific activity of 0.031 U mg^{-1}, which is 2258-fold lower than the specific activity of HodC. The behavior of the HodC-H251A protein during the purification procedure and in nondenaturing as well as denaturing PAGE was identical to that of HodC. Kinetic measurements using substrate **I** (2−200 μM) in air-saturated buffer indicated that the decrease in activity was mainly attributed to a decrease in k_{cat}^{app} (0.01 s^{-1} for **I**, compared to k_{cat}^{app} of HodC for **I** of 54 s^{-1} in air-saturated buffer). $K_{m,A}^{app}$ of the HodC-H251A protein for **I** (5.5 ± 1.2 μM) was similar to that of HodC (1.9 ± 0.4 μM), suggesting that the protein is capable of binding the organic substrate but is drastically impaired in substrate turnover.

*1H-3-Hydroxy-4-oxoquinaldine (**I**): Determination of pK_a.* The UV/vis spectra of **I** and **II** change markedly with pH, reflecting the dissociation equilibria between the protonated form, the monoanionic form, and the dianionic form. For **I**, titration from pH 1 to 3 results in shifts of the absorption maxima from 233 to 242 nm and from 321 to 334 nm with an isosbestic point at 321 nm (Figure 3A). Between pH 3 and 9, the spectra do not change (maxima at 242 and 334 nm). Titration from pH 9 to 13 leads to a bathochromic shift to maxima at 261 and 378 nm with an isosbestic point at 356 nm. Compound **II** shows a similar behavior (data not shown). Within at least 1 h, the spectra were interchangeable by adjusting the pH within the range of pH 1−13, indicating that detectable decomposition of **I** or **II** did not occur within the time of measuring. There was no difference between spectra recorded under oxic or anoxic conditions.

The pK_a values of **I** were derived from the UV/vis spectroscopic data according to Johnson and Metzler (*41*). Values of $pK_{a_1} = 1.5$ and $pK_{a_2} = 11.0$ were determined by plotting the absorbance at 334 and 305 nm and the absorbance at 372 and 334 nm, respectively, as a function of pH. The pK_a values determined experimentally for **I** are comparable to the calculated values (*42*) of 1.39 ± 0.2 and 11.01 ± 0.2. For compound **II**, the calculated values are 1.33 ± 0.2 and 10.70 ± 0.2 (*42*). At pH 8, where Hod, HodC, and Qdo show their optimum of activity, the monoanionic form of **I** and **II** prevails.

*UV/Vis Spectroscopy of Equimolar Mixtures of HodC with **I** and HodC-H251A with **I** under Anoxic Conditions.* Since the product inhibition studies suggested that the organic substrate binds to the enzyme prior to dioxygen, a mixture of the organic substrate and HodC under anoxic conditions should consist of a mixture of free enzyme (E), free substrate (A), and EA complex. Addition of equimolar amounts of

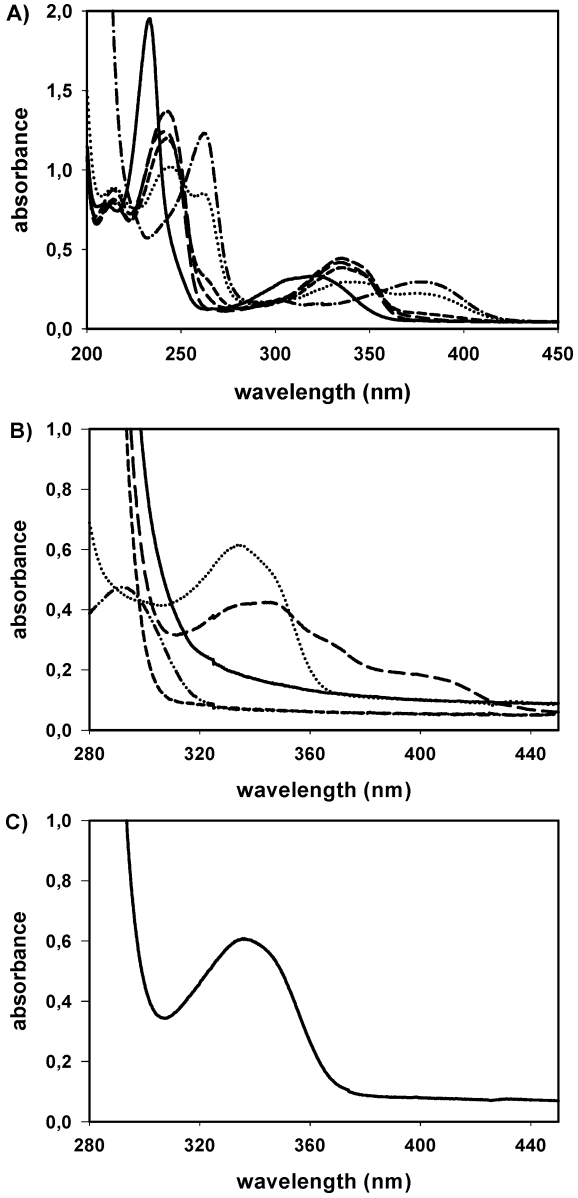

FIGURE 3: UV/vis spectra of (A) 1*H*-3-hydroxy-4-oxoquinaldine (**I**, 50 μM) at different pH values and of equimolar mixtures of (B) HodC or (C) HodC-H251A with 1*H*-3-hydroxy-4-oxoquinaldine (**I**, 50 μM each) in 50 mM Tris-HCl, pH 8.0: (A) 1*H*-3-hydroxy-4-oxoquinaldine (**I**) at pH 1 (—), pH 3 (− − −), pH 8 (- − -), pH 10 (− - -), pH 11 (···), and pH 13 (− · −); (B) HodC and **I** under oxic conditions (—), HodC and **I** under anoxic conditions (- − -), **I** (···), HodC (− - -), and *N*-acetylanthranilate (− ··); (C) HodC-H251A and **I** under anoxic conditions.

HodC to **I** at pH 8 indeed resulted in a bathochromic shift of the UV/vis spectrum (Figure 3B), suggesting that the dissociation equilibrium of **I** is shifted toward the dianion under the influence of the enzyme. The UV/vis spectrum is stable for more than 1 h and disappears immediately upon admittance of O_2. Based on the pH optimum of the 2,4-dioxygenase activity of pH 8, we suggest that free enzyme preferentially binds the substrate monoanion. Subsequently, a catalytic base in the active site of Hod may abstract a proton to form an enzyme-bound substrate dianion. Because HodC-H251A showed a drastic decrease in k_{cat}^{app} compared to HodC while $K_{m,A}^{app}$ was not altered significantly, we considered H251 a potential candidate for such a catalytic base. A mixture of equimolar amounts of HodC-H251A and

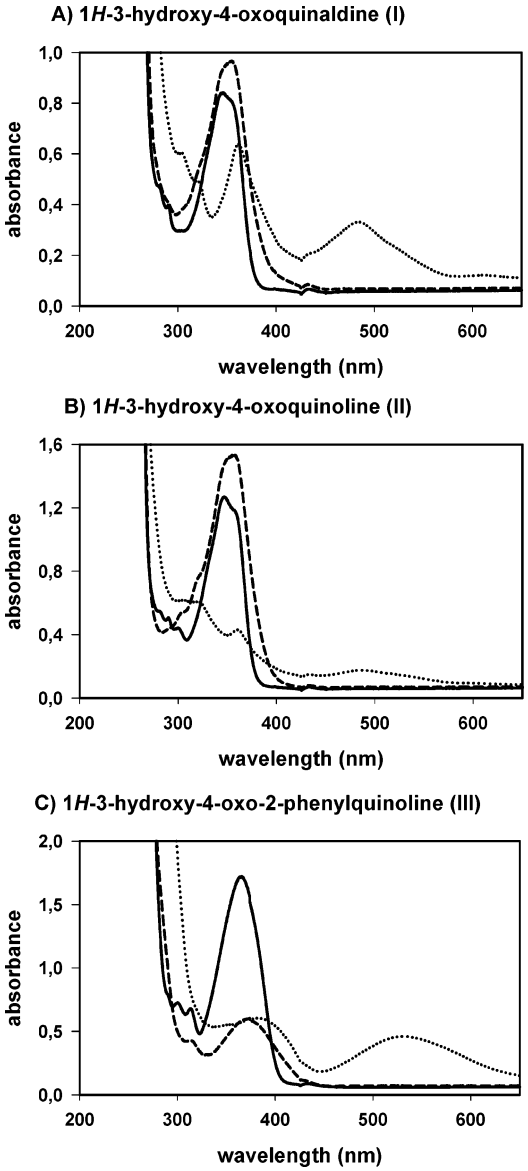

FIGURE 4: UV/vis spectra of the ^{t}BuOK-mediated chemical model reactions of (A) 1*H*-3-hydroxy-4-oxoquinaldine (**I**), (B) 1*H*-3-hydroxy-4-oxoquinoline (**II**), and (C) 1*H*-2-phenyl-3-hydroxy-4-oxoquinoline (**III**) (each 100 μM) in aprotic solvent (DMF): (—) organic compound without base; (•••) organic compound and ^{t}BuOK under oxic conditions; (— — —) organic compound and ^{t}BuOK under anoxic conditions.

I under anoxic or oxic conditions actually did not reveal the bathochromic shift typical for dianion formation of **I** (Figure 3C) but looked like the superimposed spectra of **I** at pH 8 and enzyme, indicating that the HodC-H251A protein does not catalyze measurable dianion formation. We thus suggest that upon binding of the substrate by the native enzyme, H251 in an initial step of catalysis acts as a general base to form the substrate dianion. Additional residues may be involved in activation of the organic substrate; however, H251 clearly is essential.

*UV/Vis Spectra of 1H-3-Hydroxy-4-oxoquinaldine (**I**), 1H-3-Hydroxy-4-oxoquinoline (**II**), and 1H-3-Hydroxy-4-oxo-2-phenylquinoline (**III**) in Base-Catalyzed 2,4-Dioxygenolysis.* In DMF under oxic or anoxic conditions, **I**, **II**, and **III** show absorption maxima at 345, 346, and 366 nm, respectively (Figure 4A−C). Under anoxic basic conditions (^{t}BuOK or NaOH), a bathochromic shift to 354 (**I**), 355 (**II**), and 373 nm (**III**) occurred due to deprotonation of the compounds to form the respective dianions. The spectra were stable for at least 2 h. Under basic conditions (^{t}BuOK and NaOH) and in the presence of dioxygen, all compounds transiently showed an intense red color with UV/vis spectra that showed a further bathochromic shift to 361 (**I**), 360 (**II**), and 383 nm (**III**) and additional absorption bands at 483 (**I**), 486 (**II**), and 532 nm (**III**) (Figure 4A−C). The appearance of a new band at 532 nm for **III** in the presence of dioxygen was already reported by Czaun and Speier for a mixture of 1 mmol of **III** and 1 mmol of ^{t}BuOK in 15 mL of DMF and was assigned to a 1*H*-3-hydroxy-4-oxo-2-phenylquinoline radical (*39*). We suggest that the dianions of **I** and **II**, formed by the base catalyst ^{t}BuOK, may form a radical anion by one-electron oxidation.

When the experiments were performed in aqueous solution, the spectra of **I**, **II**, and **III** also showed a bathochromic shift upon the addition of ^{t}BuOK or NaOH due to deprotonation of the monoanion. For **I**, the shift occurred from 331 to 373 nm, for **II** from 335 to 355 nm, and for **III** from 350 to 391 nm (Figure 5A−C); however, the spectra were identical under oxic and anoxic conditions (not shown). Thus, aprotic conditions appear to promote the formation of the dianions and increase their reactivity toward dioxygen, possibly due to limited reprotonation in an aprotic solvent like DMF as opposed to protic solvents. This conclusion is also supported by the catalytic constants (k_{cat}) determined for the reaction of **I** with ^{t}BuOK in DMF ($k_{cat} = 0.3\ h^{-1}$) and with ^{t}BuOK in H_2O ($k_{cat} < 0.01\ h^{-1}$).

EPR Spectroscopy of the Chemical Model Reaction and the Enzyme-Catalyzed Reaction. The reactions catalyzed by the 2,4-dioxygenases Qdo and Hod are mimicked by base-catalyzed dioxygenolysis of **I** or **II** in DMF or H_2O, using NaOH or ^{t}BuOK as catalyst (*31*, *33*). The generation of free radical species in the base-catalyzed model reaction was investigated by EPR. Since the base-catalyzed reactions proceed much more slowly than the enzyme-catalyzed conversion, EPR spectra can be recorded manually during turnover. In the following paragraphs, we mainly present the results obtained for **I** and **III** in DMF or buffer with ^{t}BuOK or NaOH as bases for which a single radical species was found throughout the time range of 3 min after preparation up to several hours. In contrast, for the model reaction of **II** at least three radical types can be observed simultaneously in variable amounts within 60 min, which additionally are quite different depending on the solvent. This prevents a clear analysis of the reactions. However, it is noted that the radical formation of **II** occurs under oxic conditions only and, in this respect, is similar to the behavior of the other substrates of the model reaction.

In anoxic equimolar mixtures of **I** or **III** with ^{t}BuOK or NaOH in aprotic conditions (DMF as solvent) or in protic conditions (buffer as solvent), no or only traces of radical signals were detected. In contrast, EPR spectra of the ^{t}BuOK-mediated model reaction with **I** or **III** in DMF in the presence of oxygen revealed clear signals of radicals. The EPR spectrum of **I** prepared under anoxic conditions in DMF shows small traces of a radical signal due to minor leakage of oxygen into the flat cell (Figure 6A). When the flat cell is opened to air for a short time a more intense eight-line pattern with resolved hyperfine structure develops (Figure 6B). Complete exposure to air for several minutes (outside

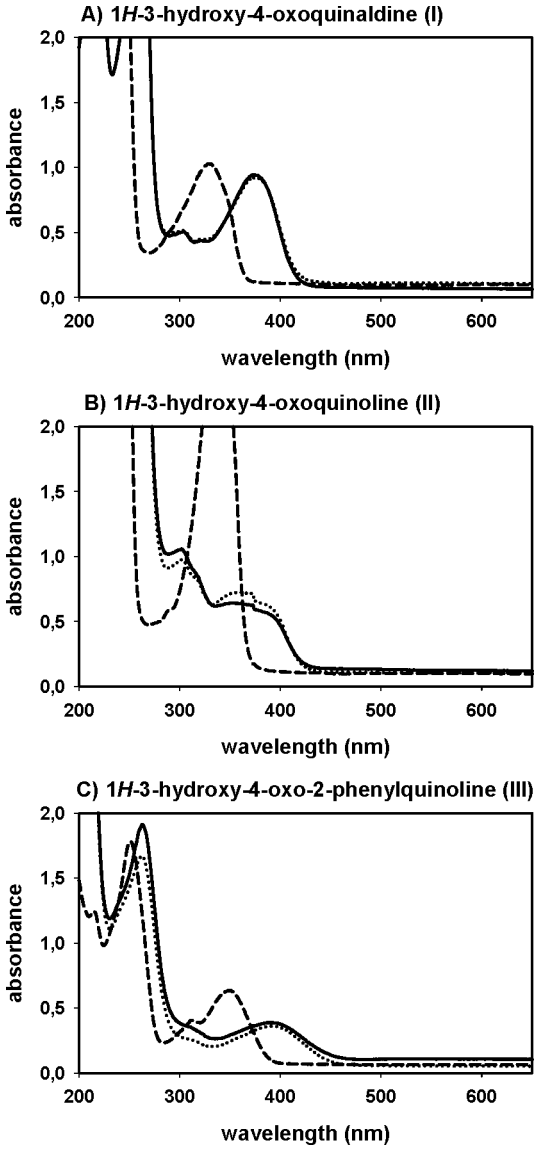

FIGURE 5: UV/vis spectra of the ^{t}BuOK- or NaOH-mediated chemical model reactions of (A) 1*H*-3-hydroxy-4-oxoquinaldine (**I**), (B) 1*H*-3-hydroxy-4-oxoquinoline (**II**), and (C) 1*H*-2-phenyl-3-hydroxy-4-oxoquinoline (**III**) (each 100 μM) in protic solvent (H_2O) under oxic conditions: (—) organic compound and NaOH; (•••) substrate and ^{t}BuOK; (– – –) substrate without base.

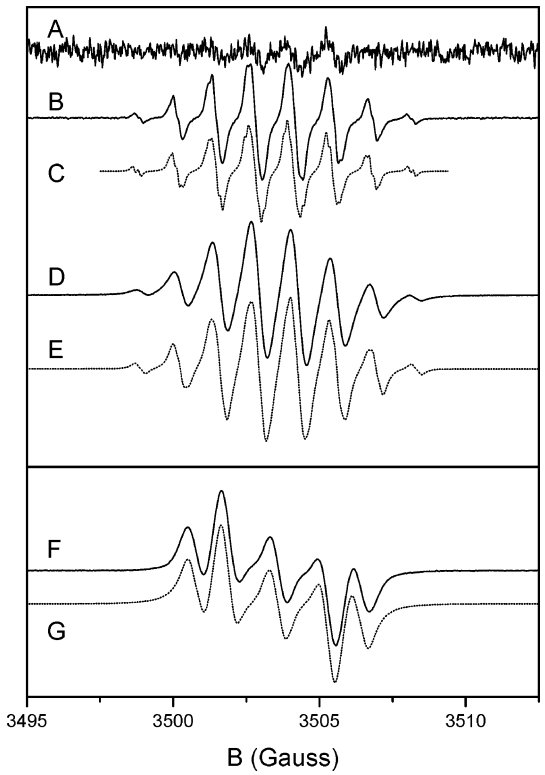

FIGURE 6: EPR spectra of the anion radicals of **I** and **III** in aprotic conditions and ^{t}BuOK as base catalyst: EPR spectra of the anion radical of **I** (A) in DMF after anoxic preparation, (B) after partial exposure to air, (C) simulation of spectrum B, (D) after exposure to air for 5 min, and (E) simulation of spectrum D; EPR spectrum of the radical of **III** (F) in DMF after exposure to oxygen and (G) its simulation. Experimental EPR parameters for spectra of **I** were 2 mW for microwave power and 0.1 G for modulation amplitude; for spectra of **III**, the microwave power was 0.2 mW and the modulation amplitude was 0.1 G.

Table 5: Simulation Parameters and Proposed Anion Radical Structures of **I** and **III**

Radical structure	Atom position	Simulation parameters[a,b]	Estimated spin densities (in %)
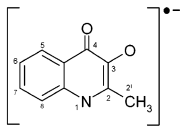	1	A(^{14}N) = 1.226G	< 1
	2^1	A(3H$_a$) = 1.345G	6
	5	A(H$_b$) = 1.440G	6
	8	A(H$_c$) = 1.475G	7
	6 or 7	A(H$_d$) = 0.170G	< 1
3,4-dioxyquinaldine radical anion (from I)		g = 2.0050	
		LW = 0.10G	
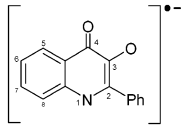	1	A(^{14}N) = 1.680G	< 1
	2	np[c]	-
	5	A(H$_a$) = 1.134G	5
	8	A(H$_b$) = 1.071G	5
	6 or 7	A(H$_d$) = 0.266G	< 1
3,4-dioxy-2-phenylquinoline radical anion (from III)		g = 2.0051	
		LW = 0.40G	

[a] In DMF. [b] 1 G = 0.1 mT. LW = line width. [c] No proton interaction present.

the flat cell) results in an intense octet EPR pattern with reduced spectral resolution (Figure 6D). This line broadening is due to interaction with paramagnetic oxygen and possibly to spin−spin interaction between the radicals. For the simulation of the hyperfine lines, an interaction of the electron spin with a nitrogen nucleus (^{14}N), three equivalent protons, two additional protons of similar coupling size, and a small proton coupling were necessary (Figure 6C, Table 5). For simulation of spectrum D, the line width was increased to 0.4 G to reproduce the line broadening. A very similar *g*-factor has been observed for the radical of **III** in DMF (*39*), which is typical for a carbon-centered radical. It is shifted from the free electron *g*-factor of 2.0023 by the influence of the spin−orbit coupling of the oxo groups of the heterocycle. Within such a radical system, isotropic hyperfine interactions are generally induced by spin polarization or hyperconjugation mechanisms with paramagnetic nuclei (^{1}H, ^{14}N) in the heterocycle **I**. The nitrogen hyperfine interaction arises from N1, and the H_a-coupling is assigned to the methyl group at C2. The protons at C5 and C8 can cause the H_b and H_c interaction, whereas the small coupling H_d may arise from N−H-proton or a further proton at the

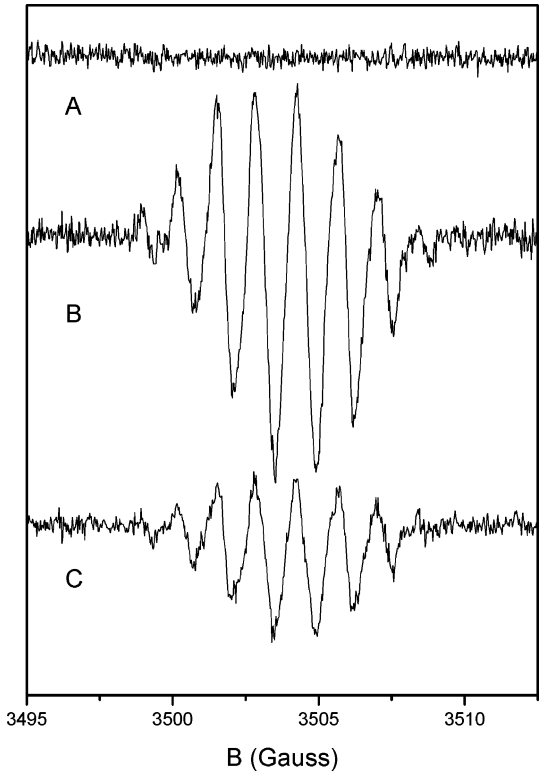

FIGURE 7: EPR spectra of the base-catalyzed (^{t}BuOK) chemical model reaction of **I** under protic conditions (Tris-HCl buffer): (A) prepared under anoxic conditions; (B) after exposure to air for 5 min; (C) in deuterated water under oxic conditions. Experimental EPR settings were 20 mW for microwave power and 0.5 G for modulation amplitude.

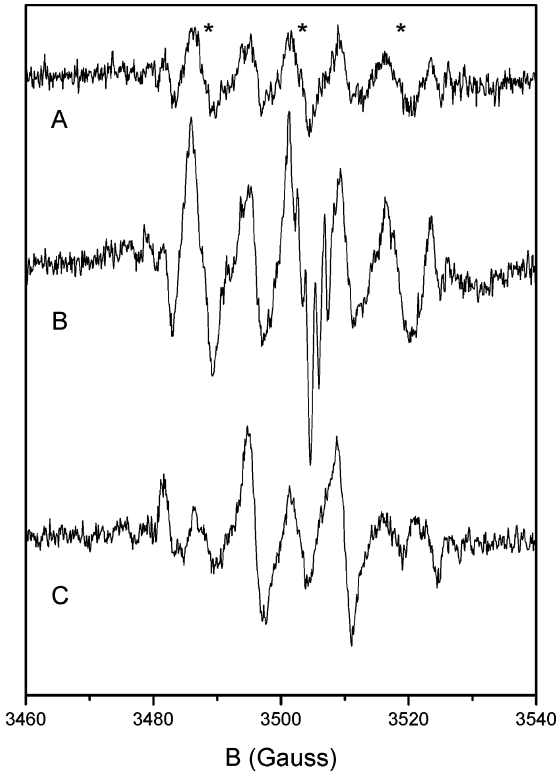

FIGURE 8: EPR spectra of (A) spin adducts of BMPO in the presence of air in Tris-HCl buffer (the asterisks indicate a triplet pattern), (B) the oxic reaction mixture of **I** and ^{t}BuOK in the presence of BMPO (the sharp lines on top of the central resonance arise from the octet pattern of Figure 7B), and (C) the enzyme and substrate in the presence of BMPO after prolonged reaction time (22 h) under oxic conditions. Experimental EPR settings were 20 mW for microwave power and 0.5 G for modulation amplitude.

adjacent six-membered ring. In the absence of isotope-substituted compounds, these assignments are consistent with the proposed structure of the 3,4-dioxoquinaldine anion radical (Table 5). For the radical anion of **III**, in which a phenyl replaces the methyl group, a more simple five line spectrum without resolved superhyperfine structure appears after exposure to dioxygen. This is in line with the lack of methyl proton interactions and can be simulated with the parameters of Table 5 in agreement with the values presented in ref *39*. Obviously, for this compound, no resolved interactions of the phenyl moiety are apparent, but the nitrogen coupling increases for this substituent as compared to **I** (Figure 6F,G).

When the environment is changed to a protic one with the aqueous buffer and ^{t}BuOK or NaOH as base catalyst, no radical signal of **I** is observed under anoxic conditions (Figure 7A). In the presence of dioxygen, the typical eight line pattern as observed in DMF appeared for **I** with ^{t}BuOK (Figure 7B) and **I** with NaOH (identical to Figure 7B), but the total signal intensity is considerably smaller (ca. 400−500-fold) than that in DMF because of the limited solubility of **I** in aqueous media. The radical signals of **I** in buffer after complete exposure to air decay in a first-order process with a characteristic time of ca. 15 min. The EPR spectra can be well fitted with parameters very close to those determined for **I** in DMF (Table 5). The small changes in hyperfine couplings (±0.05 G) are related to the difference in solvent polarity. When the experiments are performed in D_2O, an identical eight line signal is recorded showing no change in line width or splitting of lines (Figure 7C). This indicates that no exchangeable proton, that is, at N1, is involved. This result is supported by the finding that **III** and ^{t}BuOK in the presence of air show exactly the same EPR spectra in buffer and in D_2O. It is concluded that the smallest hyperfine interaction probably arises from a proton at C6 or C7. At least for the aqueous system, the N1 position remains deprotonated in the radical state, which is consistent with the dianionic forms of **I** (and **II** and **III**) prevailing under the applied strong basic conditions (pH > 13) and is in line with the pK_a values of ∼11 for the dissociation of the second proton (this work, *42*) as suggested by the UV/vis absorption spectra (see above).

The EPR data support the hypothesis that the dianion of the substrates is the reactive catalytic intermediate that undergoes radical formation. The dianion of **I** (as well as of **II** and **III**) might activate dioxygen by single-electron transfer (SET) to form superoxide. We attempted to detect superoxide anion radicals by using the spin trap BMPO (*43*). In the absence of oxygen, the reaction mixture and the control experiments (buffer + BMPO, **I** + BMPO, ^{t}BuOK + BMPO) show only very weak signals even after long accumulation times. However, under oxic conditions clear signals were already found in control experiments, one of which is shown in Figure 8A for buffer + BMPO. From a comparison of the control experiments, the apparent lines are assigned to two groups, a triplet (marked by asterisks) and a quartet. The latter is associated with an OH or OOH adduct of BMPO on the basis of its splitting (*43*), whereas the origin of the triplet is presently unclear. Obviously, some

spontaneous radical formation and trapping is occurring in the controls under these conditions. For the reaction mixture **I** with ^{t}BuOK and BMPO, a similar line pattern with a 2- or 3-fold enhanced intensity was observed. In addition, on the central line the typical eight line pattern of radical **I** is visible, indicating the coexistence of trapped BMPO radicals and the carbon-centered radical of **I** (Figure 8B, compare Figure 7). It has to be stated that the rather complex composition of the trapping experiment, the spontaneous radical formation, and the unknown kinetics and reaction pathways of different types of radicals do not allow us to conclude clearly on the trapping of superoxide (or its products) generated in a SET process.

Nevertheless, similar experiments were performed on the enzyme, the substrate **I**, and mixtures of HodC and **I** under anoxic and oxic conditions, each in the presence and absence of the spin trap BMPO. Without the spin trap, no radical signals at all were detected. In the presence of BMPO, apart from spontaneously formed "background signals" already seen in control experiments, no clear indication of radicals originating from the enzyme reaction is found. In one case after a prolonged reaction time (22 h) of the enzyme mixture, the spectrum in Figure 8C was recorded, again showing the triplet signal and an enhanced quartet pattern. It is, however, not possible to correlate the latter signal to trapped activated oxygen species arising from the enzyme reaction. Thus, free enzyme and free substrate do not contain any stable paramagnetic radical species under anoxic or oxic conditions. On the basis of the present database, it cannot be excluded that a spin-coupled, EPR-silent radical pair in the anoxic ES complex or during catalysis is formed or that short-lived free radicals are generated in the catalytic cycle. Two reasons may explain the failure of the trapping experiments: first, the site of radical formation in the protein matrix may be inaccessible for the spin trap, and second, the trapping rate may be slower than other possible reaction pathways for the radical. For the detection of short-lived free radicals that occur transiently during catalysis, stopped-flow EPR techniques might be more appropriate.

DISCUSSION

HodC-catalyzed dioxygenolysis proceeds via a compulsory-order ternary-complex mechanism, where the organic substrate binds prior to dioxygen, and CO leaves the enzyme−product complex first, followed by the organic product. To explain ordered substrate binding, one may assume that either the substrate that binds first induces a conformational change that is necessary to allow access or binding of the second substrate or the second substrate interacts directly with the enzyme-bound first substrate without any need to bind to the enzyme. In the case of riboflavin kinase, for instance, multiple conformational changes that are induced by substrate binding and product release were suggested to be the rationale for its ordered kinetic mechanism (*44*). For the flavin-dependent bacterial luciferase, nitroalkane oxidase, and cholesterol oxidase, conformational changes during catalysis are thought to be a prerequisite for the reaction of the reduced flavin with dioxygen (*45*−*47*). Structural dynamics along the reaction coordinate also was proposed for several members of the α/*β*-hydrolase fold family of enzymes (*48*−*50*). Alternatively (or additionally), the compulsory order of substrate binding found for HodC might be explained by a mechanism where dioxygen neither binds to nor reacts with the enzyme but is directly "trapped" by the activated substrate of the ES complex. Such a reaction in fact has been discussed for other, evolutionary unrelated, oxygenases, such as lipoxygenase, which was proposed to catalyze the direct reaction of dioxygen with an enzyme-bound substrate radical generated by hydrogen abstraction (*51*, *52*).

In HodC, activation of the organic substrate in a first step in catalysis involves dianion formation by H251 as a general base (Scheme 3, step 1). Remarkably, this histidine residue aligns with the triad histidine of the α/*β* hydrolases. Our data show that enzyme-catalyzed proton abstraction from the

Scheme 3: Postulated Reaction Sequence of 2,4-Dioxygenolysis Catalyzed by Hod

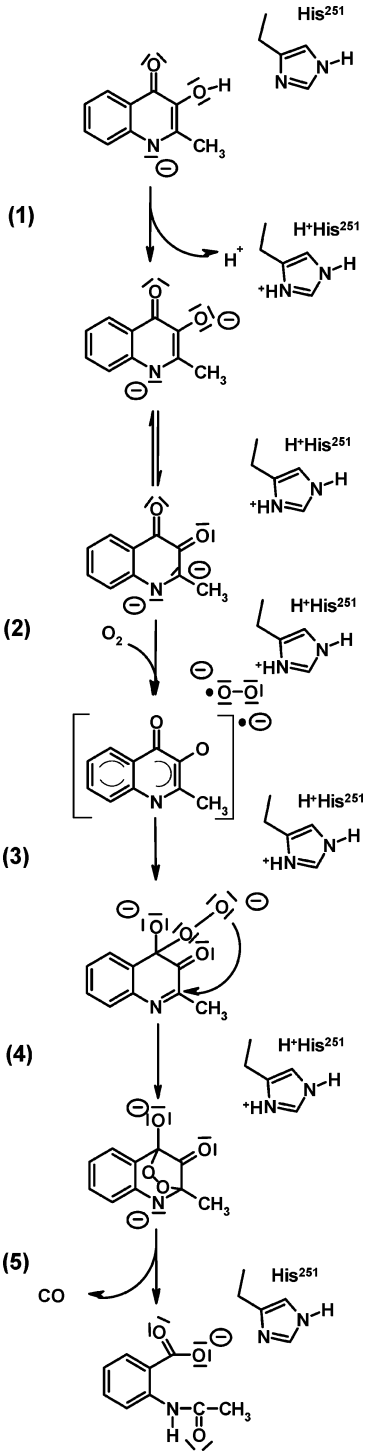

substrate monoanion occurs independently of the presence of dioxygen; it probably even is a prerequisite for the subsequent reaction with dioxygen. Substrate activation in advance to dioxygen binding actually appears to be a common theme in a number of O_2-dependent enzymes. The most intriguing examples are the ActVA-Orf6 protein and urate oxidase, because they also lack a cofactor to participate in the catalytic reaction with dioxygen. Urate oxidase was shown to generate the urate dianion as the first catalytic intermediate (*9*, *53*). Providing a general base to generate the urate dianion is in fact thought to be the key role of the enzyme, because oxidation of the urate dianion is more facile than oxidation of the monoanion (*11*). By analogy, we assume that the enzyme-bound dianion of **I** or **II** directly transfers a single electron to dioxygen (Scheme 3, step 2). Single-electron oxidation to form a radical anion of **I** actually was observed in the chemical model reaction (cf. Figure 7). In addition to acting as a general base to generate the dianion, H251 of Hod in its protonated form may take over further roles in catalysis. It is interesting to point out that in the flavoprotein glucose oxidase, a conserved histidine is largely responsible for catalyzing the reaction between $FADH^-$ and O_2, as protonation of this histidine creates a polarized environment that is optimal for electron transfer to O_2 (*54*). Theoretical calculations suggested that the electron affinity of dioxygen in the presence of a protonated histidine is extremely high (*55*, *56*). If in the ternary complex [Hod−substrate dianion−O_2] the dioxygen molecule indeed is positioned in close proximity to this residue, $H251H^+$ thus may be crucial for dioxygen reduction.

A productive reaction pathway via single-electron transfer requires substrates that can form resonance-stabilized radicals. The ability of the reduced flavins, pterins, and urate anion to delocalize and thus stabilize an unpaired electron is known to be important for their facile reaction with O_2. This property also seems to be inherent to the radical anions of **I**, **III**, and, by analogy, **II** observed in base-catalyzed chemical dioxygenolysis. The spectral simulations of hyperfine interactions found for the radicals of **I** and **III** in the model reaction are indicative for a spin delocalization over the asymmetric ring systems. In particular, it becomes apparent that the substituent (methyl or phenyl group) at position 2 affects the spin distribution, which can be inferred from the increase of the N1 interaction with concomitant decrease of the coupling to protons at positions 5 and 8 upon going from **I** to **III** (Table 5). The presence of a sizable hyperfine interaction of the methyl protons is consistent with a considerable spin density at the C2 position. For a freely rotating methyl group in β-position to C2, a spin density of about 6% can be estimated to reside on C2. For C5 and C8, corresponding values of 6−7% are obtained, whereas the spin density at N1 appears to be rather small (<1%) (*57*, *58*). Although these calculated values for spin distribution represent only rough estimates in the absence of isotope substitution experiments and ab initio calculations for the compounds used, it appears that about 20% of the unpaired spin is distributed asymmetrically to these positions of the heterocycles (Table 5). The major part of the spin density is then located at C4, C3, or both. A distinction between these sites would require specific isotope labeling (e.g., with ^{13}C and ^{17}O).

However, in contrast to the chemical model reaction, radical species could not be detected in the enzyme-catalyzed reaction by means of spin trapping and EPR spectroscopy. We nevertheless suggest that single-electron transfer from the resonance-stabilized substrate dianion to dioxygen may occur in the ternary complex, resulting in a caged radical pair (Scheme 3, step 2). Caged radical pairs due to spin coupling are not detectable by conventional EPR, nor are they accessible to spin trapping agents.

Further along the reaction coordinate, the radical pair generated by electron transfer from the organic donor molecule to dioxygen has to undergo a triplet to singlet spin transition for the subsequent radical recombination to occur. With respect to the radical reaction, the formation of a C4-hydroperoxy(di)anion thus seems plausible (Scheme 3, step 3). In the case of the enzyme-catalyzed reaction, it is however not known whether electron-coupled proton transfer occurs from the protonated histidine in this step. Subsequent intramolecular attack of the C4-hydroperoxy(di)anion on C2 would result in the 2,4-endoperoxy(di)anion (Scheme 3, step 4). Its decomposition with cleavage of one O−O and two C−C bonds (and reprotonation) would yield carbon monoxide and *N*-acetylanthranilate (from **I**) or *N*-formylanthranilate (from **II**) (Scheme 3, step 5). However, the considerable spin density on C2 might enable an alternative pathway starting with the formation of a C2-hydroperoxy(di)anion, which also would collapse into the products via the 2,4-endoperoxy(di)anion. The proposed hydroperoxy(di)anion and the 2,4-endoperoxy(di)anion intermediates have not yet been experimentally verified. However, previous $(^{18}O)O_2/(^{16}O)O_2$ incorporation experiments performed with Hod and Qdo indicated insertion of both oxygen atoms of a single O_2 molecule into the respective organic product; one of the oxygen atoms was assigned to the carboxyl group and the other to the formyl or acetyl group of the respective organic product (*33*). This result together with the failure to detect any products other than CO and *N*-acetyl- or *N*-formylanthranilate in the enzyme-catalyzed reactions exclude the possibility of a dioxetane instead of a 2,4-endoperoxide intermediate.

In conclusion, besides activating the substrate 1*H*-3-hydroxy-4-oxoquinaldine through the active site base, the function of Hod may be to provide aprotic, low-dielectric reaction conditions and an environment that is optimal for electron transfer. The enzyme also may electrostatically stabilize anionic transition states, intermediates, or both and sequester intermediates from side reactions.

Oxygenases without requirement for cofactors or metal ions present considerable interest in terms of fundamental chemical biology and in terms of enzyme evolution. We suggest that a common feature of these enzymes may be the fact that they all catalyze the dioxygenation of an organic substrate that easily undergoes a one-electron oxidation to form a resonance-stabilized radical. However, elucidation of the catalytic role of the scaffold of the α/β hydrolase fold in dioxygenolysis has to await further studies.

ACKNOWLEDGMENT

We thank Renate Gahl-Janssen for numerous protein preparations and expert technical assistance. We thank B.

Kalyanaraman, The Medical College of Wisconsin, Milwaukee, WI, for the generous gift of BMPO, and T. D. H. Bugg (University of Warwick, U.K.) and R. A. Steiner (European Oncology Institute, Milan, Italy) for stimulating discussions.

REFERENCES

1. Fetzner, S. (2002) Oxygenases without requirement for cofactors or metal ions, *Appl. Microbiol. Biotechnol. 60*, 243−257.
2. Fischer, F., Künne, S., and Fetzner, S. (1999) Bacterial 2,4-dioxygenases: new members of the α/*β* hydrolase-fold superfamily of enzymes functionally related to serine hydrolases, *J. Bacteriol. 181*, 5725−5733.
3. Hotelier, T., Renault, L., Cousin, X., Negre, V., Marchot, P., and Chatonnet, A. (2004) ESTHER, the database of the alpha/beta-hydrolase fold superfamily of proteins, *Nucleic Acids Res. 32*, D145−D147.
4. Nardini, M., and Dijkstra, W. (1999) α/*β* Hydrolase fold enzymes: the family keeps growing, *Curr. Opin. Struct. Biol. 9*, 732−737.
5. Holmquist, M. (2000) Alpha/beta-hydrolase fold enzymes: structures, functions and mechanisms, *Curr. Protein Pept. Sci. 1*, 209−235.
6. Matthews, J. C., Hori, K., and Cormier, M. J. (1977) Purification and properties of *Renilla reniformis* luciferase, *Biochemistry 16*, 85−91.
7. Lorenz, W. W., McCann, R. O., Longiaru, M., and Cormier, M. J. (1991) Isolation and expression of a cDNA encoding *Renilla reniformis* luciferase, *Proc. Natl. Acad. Sci. U.S.A. 88*, 4438−4442.
8. Fischer, F., and Fetzner, S. (2000) Site-directed mutagenesis of potential catalytic residues in 1*H*-3-hydroxy-4-oxoquinoline 2,4-dioxygenase, and hypothesis on the catalytic mechanism of 2,4-dioxygenolytic ring cleavage, *FEMS Microbiol. Lett. 190*, 21−27.
9. Kahn, K., and Tipton, P. A. (1998) Spectroscopic characterization of intermediates in the urate oxidase reaction, *Biochemistry 37*, 11651−11659.
10. Sarma, A. D., and Tipton, P. A. (2000) Evidence for urate hydroperoxide as an intermediate in the urate oxidase reaction, *J. Am. Chem. Soc. 122*, 11252−11253.
11. Tipton, P. A. (1999) Kinetic studies of urate oxidase, in *Enzymatic Mechanisms* (Frey, P. A., and Northrop, D. B., Eds.) pp 278−287, IOS Press, Amsterdam, Netherlands.
12. Sciara, G., Kendrew, S. G., Miele, A. E., Marsh, N. G., Federici, L., Malatesta, F., Schimperna, G., Savino, C., and Vallone, B. (2003) The structure of ActVA-Orf6, a novel type of monooxygenase involved in actinorhodin biosynthesis, *EMBO J. 22*, 205−215.
13. Bugg, T. D. H. (2001) Oxygenases: mechanisms and structural motifs for O_2 activation, *Curr. Opin. Chem. Biol. 5*, 550−555.
14. Bruice, T. C. (1984) Oxygen-flavin chemistry, *Isr. J. Chem. 24*, 54−61.
15. Palfey, B. A., Ballou, D. P., and Massey, V. (1995) Oxygen activation by flavins and pterins, in *Active Oxygen in Biochemistry* (Valentine, J. S., Foote, C. S., Greenberg, A. and Liebman, J. F., Eds.) pp 37−83, Blackie Academic and Professional (Chapman and Hall), London.
16. Goto, T. (1968) Chemistry of bioluminescence, *Pure Appl. Chem. 17*, 421−441.
17. Abell, L. M., and Schloss, J. V. (1991) Oxygenase side reactions of acetolactate synthase and other carbanion-forming enzymes, *Biochemistry 30*, 7883−7887.
18. Eiden, D., Wendt, R., and Fenner, H. (1978) Chinolyliden-Derivate, *Arch. Pharm. (Weinheim, Ger.) 311*, 561−568.
19. Cornforth, J. W., and James, A. T. (1956) Structure of naturally occurring antagonist of dihydrostreptomycin, *Biochem. J. 63*, 124−130.
20. Evans, D. J., and Eastwood, F. W. (1974) Synthesis of an arylhydroxytetronimide and of 3-hydroxy-(1*H*)-quinolone derivatives, *Aust. J. Chem. 27*, 537−542.
21. Harris, R. L. N. (1976) Potential wool growth inhibitors. Improved synthesis of mimosine and related 4(1*H*)-pyridones, *Aust. J. Chem. 29*, 1329−1334.
22. Nelson, W. O., Karpishin, T. B., Rettig, S. J., and Orvig, C. (1988) Physical and structural studies of *N*-substituted-3-hydroxy-2-methyl-4(1*H*)-pyridinones, *Can. J. Chem. 66*, 123−131.
23. Hradil, P., Hlaváč, J., and Lemr, K. (1999) Preparation of 1,2-disubstituted-3-hydroxy-4(1*H*)-quinolinones and the influence of substitution on the course of cyclization, *J. Heterocycl. Chem. 36*, 141−144.
24. Szczepankiewicz, W., and Suwinski, J. (2000) One-pot synthesis of 3-(2-cyanophenyl)quinazolin-4(3*H*)-one, *Chem. Heterocycl. Compd. (N. Y.) 36*, 809−810.
25. IUPAC, Commission on Nomenclature of Organic Chemistry (1993) *A Guide to IUPAC Nomenclature of Organic Compounds (Recommendations 1993)* (Panico, R., Powell, W. H., and Richer, J.-C. (senior editor), Eds.) Blackwell Scientific publications, Oxford, U.K.
26. Dembek, G., Rommel, T., Lingens, F., and Höke, H. (1989) Degradation of quinaldine by *Alcaligenes* sp. and by *Arthrobacter* sp., *FEBS Lett. 246*, 113−116.
27. Sambrook, J., Fritsch, E. F., and Maniatis, T. (1989) *Molecular Cloning: A Laboratory Manual*, Cold Spring Harbor Laboratory Press, Cold Spring Harbor, NY.
28. Jerpseth, B., Greener, A., Short, J. M., Viola, J., and Kretz, P. L. (1992) XL1-Blue MRF′ *E. coli* cells: *mcrA*$^-$, *mcr*CB$^-$, *mcr*F$^-$, *mrr*$^-$, *hsd*R$^-$ derivative of XL1-Blue cells, *Strategies Mol. Biol. 5*, 81−83.
29. Iwasaki, K., Uchiyama, H., Yagi, O., Kurabayashi, T., Ishizuku, K., and Takamury, Y. (1994) Transformation of *Pseudomonas putida* by electroporation, *Biosci. Biotech. Biochem. 58*, 851−854.
30. Hopwood, D. A., Bibb, M. J., Chater, K. F., Kieser, T., Burton, C. J., Kieser, H. M., Lydiate, D. J., Smith, C. P., Ward, J. M., and Schrempf, H. (1985) *Genetic Manipulation of Streptomyces: A Laboratory Manual*, The John Innes Foundation, Norwich, England.
31. Fischer, F. (2000) Molekulargenetische und biochemische Untersuchungen zum Reaktionsmechanismus Cofaktor-freier 2,4-Dioxygenasen, Ph.D. Thesis, University of Oldenburg, Germany.
32. Dower, W. J., Miller, J. F., and Ragsdale, C. W. (1988) High efficiency transformation of *E. coli* by high voltage electroporation, *Nucleic Acids Res. 16*, 6127−6145.
33. Bauer, I., Max, N., Fetzner, S., and Lingens, F. (1996) 2,4-Dioxygenases catalyzing *N*-heterocyclic-ring cleavage and formation of carbon monoxide. Purification and some properties of 1*H*-3-hydroxy-4-oxoquinaldine 2,4-dioxygenase from *Arthrobacter* sp. Rü61a and comparison with 1*H*-3-hydroxy-4-oxoquinoline 2,4-dioxygenase from *Pseudomonas putida* 33/1, *Eur. J. Biochem. 240*, 576−583.
34. Hames, B. D. (1990) One-dimensional polyacrylamide gel electrophoresis, in *Gel Electrophoresis of Proteins*, 2nd ed. (Hames, B. D. and Rickwood, D., Eds.) pp 1−147, IRL press, Oxford, U.K.
35. Zor, T., and Selinger, Z. (1996) Linearisation of the Bradford protein assay increases its sensitivity: Theoretical and experimental studies, *Anal. Biochem. 236*, 302−308.
36. Hitchman, M. L. (1978) Measurement of dissolved oxygen, in *Chemical Analysis, A Series of Monographs on Analytical Chemistry and its Applications* (Elving, P. J., and Winefordner, J. D., Eds.) Vol. 49, pp 200−210, John Wiley and Sons, New York.
37. Budavari, S., Ed. (1989) *The Merck Index*, 11th ed, Merck & Co. Inc., Rahway, NJ.
38. Cornish-Bowden, A. (1995) *Analysis of enzyme kinetic data*, Oxford University Press, New York.
39. Czaun, M., and Speier, G. (2002) The base-catalyzed oxygenation of quinoline derivatives, *Tetrahedron Lett. 43*, 5961−5963.
40. Rudolph, F. B. (1979) Product inhibition and abortive complex formation, *Methods Enzymol. 63*, 411−436.
41. Johnson, R. J., and Metzler, D. E. (1970) Analyzing the spectra of Vitamin B_6 derivatives, *Methods Enzymol. 18A*, 433−471.
42. Advanced Chemistry Development (ACD) Software Solaris V4.67 ((C) 1994−2001 ACD) SCIFI (Scientific Finder Scholar).
43. Zhao, H., Joseph, J., Zhang, H., Karoui, H., and Kalyanaraman, B. (2001) Synthesis and biochemical applications of a solid cyclic nitrone spin trap: A relatively superior trap for detecting superoxide anions and glutathiyl radicals, *Free Radical Biol. Med. 31* (5), 599−606.
44. Karthikeyan, S., Zhou, Q., Osterman, A. L., and Zhang, H. (2003) Ligand binding-induced conformational changes in riboflavin kinase: structural basis for the ordered mechanism, *Biochemistry 42*, 12532−12538.

45. Abu-Soud, H., Mullins, L. S., Baldwin, T. O., and Raushel, F. M. (1992) Stopped-flow kinetic analysis of the bacterial luciferase reaction, *Biochemistry 31*, 3807−6812.
46. Gadda, G., and Fitzpatrick, P. F. (2000) Iso-mechanism of nitroalkane oxidase: 1. Inhibition studies and activation by imidazole, *Biochemistry 39*, 1400−1405.
47. Coulombe, R., Yue, K. Q., Ghisla, S., and Vrielink, A. (2001) Oxygen access to the active site of cholesterol oxidase through a narrow channel is gated by an Arg-Glu pair, *J. Biol. Chem. 27*, 30435−30441.
48. Lawson, D. M., Brzozowski, A. M., Rety, S., Verma, C., and Dodson, G. G. (1994) Probing the nature of substrate binding in *Humicola lanuginosa* lipase through X-ray crystallography and intuitive modeling, *Protein Eng. 7*, 543−550.
49. Gunasekaran, K., Ma, B., and Nussinov, R. (2003) Triggering loops and enzyme function: Identification of loops that trigger and modulate movements, *J. Mol. Biol. 332*, 143−159.
50. Schanstra, J. P., and Janssen, D. B. (1996) Kinetics of halide release of haloalkane dehalogenase: evidence for a slow conformational change, *Biochemistry 35*, 5624−5632.
51. Glickman, M. H., and Klinman, J. P. (1996) Lipoxygenase reaction mechanism: Demonstration that hydrogen abstraction from substrate precedes dioxygen binding during catalytic turnover, *Biochemistry 35*, 12882−12892.
52. Knapp, M. J., and Klinman, J. P. (2003) Kinetic studies of oxygen reactivity in soybean lipoxygenase-1, *Biochemistry 42*, 11466−11475.
53. Imhoff, R. D., Power, N. P., Borrok, M. J., and Tipton, P. A. (2003) General base catalysis in the urate oxidase reaction: Evidence for a novel Thr-Lys catalytic diad, *Biochemistry 42*, 4094−4100.
54. Roth, J. P., and Klinman, J. P. (2003) Catalysis of electron transfer during activation of O_2 by the flavoprotein glucose oxidase, *Proc. Natl. Acad. Sci. U.S.A. 100*, 62−67.
55. Prabhakar, R., Siegbahn, P. E. M., Minaev, B. F., and Ågren, H. (2002) Activation of triplet dioxygen by glucose oxidase: spin−orbit coupling in the superoxide ion, *J. Phys. Chem. B 106*, 3742−3750.
56. Prabhakar, R., Siegbahn, E. M., and Minaev, B. F. (2003) A theoretical study of the dioxygen activation by glucose oxidase and copper amine oxidase, *Biochim. Biophys. Acta 1647*, 173−178.
57. McConnell, H. M. (1956) Indirect hyperfine interactions in the paramagnetic resonance spectra of aromatic free radicals, *J. Chem. Phys. 24*, 764−766.
58. McConnell, H. M., and Chesnut, D. B. (1985) Theory of isotropic hyperfine interactions in π-electron radicals, *J. Chem. Phys. 28*, 107−117.

BI048735U